Ultrahigh-contrast-ratio silicon Fano diode

W. Ding,[1] B. Luk'yanchuk,[2,*] and C.-W. Qiu[1,†]

[1]*Department of Electrical and Computer Engineering, National University of Singapore, 4 Engineering Drive 3, Singapore 117576*

[2]*Data Storage Institute, Agency for Science, Technology, and Research, Engineering Drive 1, Singapore 117608*

(Received 27 September 2011; published 27 February 2012)

We report a distinguished mechanism of using two interaction-free (uncoupled) cavities to realize an all-optical silicon diode with an extremely high contrast ratio. In contrast to existing examples of all-optical diodes, our unidirectional transmission results from mimicking Fano resonance in a compact and finite silicon waveguide. A Fano spectrum with an arbitrary asymmetric factor, resonant center, and linewidth is explicitly designed with two symmetric resonances, which can be separately realized and tuned in an insightful manner by two cascaded uncoupled cavities. The field localizations are inherently asymmetric. We show that if these double asymmetries (Fano spectrum and field localization) are integrated and controlled, an ultrahigh-contrast-ratio silicon Fano diode is accomplished. This finding provides a promising avenue for achieving an extremely compact optical switch and incorporating Fano resonance in silicon photonics.

DOI: 10.1103/PhysRevA.85.025806 PACS number(s): 42.65.Pc, 42.70.Qs

The optical diode (OD), which allows light to propagate along one direction only (e.g., from right to left; "RL") and blocks the transmission for the other direction (from left to right; "LR"), has attracted much attention for its important roles in optical systems. Up to now, many different mechanisms and methods to achieve ODs have been proposed, such as using metamaterials [1,2], tunable liquid crystals [3], nonreciprocal loss [4], Mach-Zehnder interferometers [5], cascaded gratings [6], nonlinear harmonic generation [7], indirect interband photonic transitions [8], and ferromagnetic structures [9–14]. The all-optical diode (AOD) is still being investigated for its advantages in all-optical operation, short relaxing time, and compactness. One can use multilayer structures with gradually changed refractive index distribution [15,16], quasiperiodic one-dimensional (1D) photonic crystals [17–20], nonlinear cavities with different confinement strengths along the left and right sides [21,22], or two coupled nonlinear cavities [23,24].

In spite of the merits of AOD structures, the transmission contrast C is usually low. Here the transmission contrast ratio $C(I_i) = I_{\mathrm{RL}}/I_{\mathrm{LR}}$ is the ratio of the transmission intensities for LR and RL operations at the same incident level of I_i. This low C is inherently determined by the Lorentzian spectrum shape of the AOD structure, as illustrated in Fig. 1(a), which is widely adopted in the investigation of AODs. One may argue that it is possible to make the transmission of one direction nearly zero, resulting in an infinite C. However, under such circumstance, the transmission along the other direction usually becomes very small too, which in turn restricts realistic application. To overcome this intrinsic problem, we propose a distinguished schematic for AODs based on manipulating Fano-shaped transmission spectra [25–27] which simultaneously demonstrates a contrast ratio of $C \sim \infty$ in principle and high unidirectional transmission. This high contrast ratio is mainly due to $T_{\mathrm{LR}}(\omega_i)$ located at the zero point of the Fano-resonant line shape. More importantly, a rather high transmission T_{RL} along the RL direction is maintained at this frequency (more than 0.7), and the nonlinear shift of the spectrum is much smaller compared to those of Lorentzian AODs.

Fano resonance, which is characterized by an asymmetric line shape, is a universal phenomenon throughout physics [25]. In photonics, Fano resonances have been widely investigated in nano plasmonic structures [27–33] and dielectric or semiconductor systems [26,34], such as photonic crystals (PCs) [35–37], slabs [38,39], photoemitters [40], indirect coupling cavities [41], and coupled cavity systems [42–44].

Hence, our Brief Report exploits the principle of Fano resonance to manipulate the Fano factor, resonant center, and linewidth [45] in a finite silicon waveguide in order to solve the aforementioned problem of the AOD. In this case, we decompose and redesign the silicon waveguide to achieve the desired Fano resonance using "multiplication interpretation" and find that a Fano line with desired parameters can be easily tailored in a very compact way. Our designs also demonstrate that the field localization is inherently asymmetrical when the same signal is fed from opposite directions. The cooperation of these two asymmetries (Fano spectrum and field localization) provides an extremely efficient mechanism for unidirectional transmission or all-optical diode (AOD) operation. A transmission contrast ratio tending to infinity is predicted and verified. Note that the state-of-the-art AODs based on Lorentzian lines can achieve the contrast ratio C on the order of 10 (e.g., 20 in Ref. [18], 4.2 in Ref. [19], 3 in Ref. [21], 30 in Ref. [22], and 10 in Ref. [23]). Therefore, our design mechanism based on Fano lines demonstrates significant improvement of the contrast ratio.

Fano transmission spectrum $T(\omega)$ can be characterized

$$T(\omega) = T_0 \frac{(\epsilon + f)^2}{\epsilon^2 + 1} \quad \text{with} \quad \epsilon = \frac{2(\omega - \omega_0)}{\Gamma}. \tag{1}$$

Here ω, ω_0, and Γ are the signal frequency, resonance center, and resonance linewidth, respectively. f is the Fano factor that determines the degree of asymmetry. We show that a standard

*boris_l@dsi.a-star.edu.sg

†To whom correspondence should be sent: eleqc@nus.edu.sg

 ©2012 American Physical Society

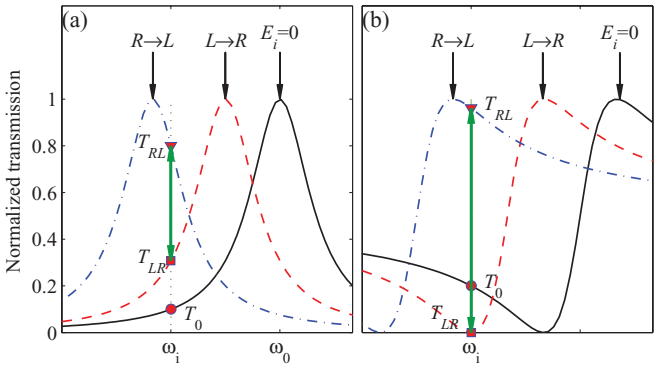

FIG. 1. (Color online) Principle illustration of the high-transmission-contrast-ratio silicon Fano diode (SFD). ω_i is the operation frequency. Solid, dash-dotted, and dashed lines show the transmission spectra of linear case, nonlinear left to right (LR), and nonlinear right to left (RL) operations, respectively. (a) For a Lorentzian-shaped spectrum. (b) For a Fano-shaped spectrum.

Fano line can be decomposed into the product of a Lorentzian line and a parabolic line

$$T(\omega) = T_1 T_2 = \frac{(\Gamma/2)^2}{(\Gamma/2)^2 + (\omega - \omega_0)^2} \left[\frac{\omega - (\omega_0 - f\Gamma/2)}{\Gamma/2} \right]^2. \tag{2}$$

The term T_1 is a standard symmetrical Lorentzian line centered at $\omega_{10} = \omega_0$ with a linewidth of Γ. The term T_2 is a parabolic line with a symmetrical center of $\omega_{20} = \omega_0 - f\Gamma/2$ with a linewidth of Γ [which is the frequency separation between ω_a and ω_b from $T_2(\omega_{a,b}) = 1$].

In Fig. 2, we plot T_1, T_2, and T for $f = 0$, 1, -1, and 3 in (a), (b), (c), and (d), respectively. In the frequency ranges where T_1 and T_2 both are increasing (decreasing) with ω, a rapid increase (decrease) in the spectrum is formed. In other ranges, however, T_1 and T_2 change conversely (one is increasing and the other is decreasing), which results in relatively slow changes in the spectrum. Finally, a Fano line

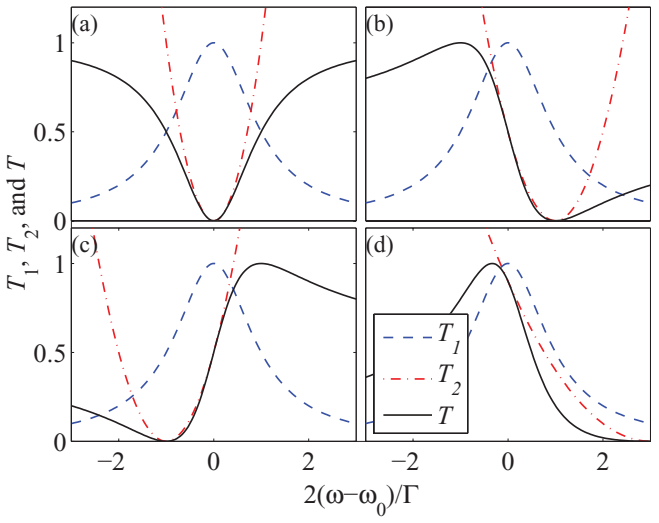

FIG. 2. (Color online) Decomposition of a Fano line T (solid) into two symmetrical ones of T_1 (dashed) and T_2 (dash dotted) according to Eq. (2). (a) $f = 0$. (b) $f = 1$. (c) $f = -1$. (d) $f = 3$.

with the character of asymmetry is formed. On the other hand, when two elements with response functions of T_1 and T_2 are designed separately and then cascaded together according to Eq. (2), a Fano-shaped line will be obtained. This is the most fundamental physics for the design of the proposed Fano diode.

In Eq. (2), the parameters of T_1 and T_2, such as the central frequencies and the linewidths, appear to be dependent on each other. Nevertheless, these parameters can be independent of each other in general. Based on this point, Eq. (2) is extended to the form of

$$T = T_1 T_2 = \frac{(\Gamma_1/2)^2}{(\Gamma_1/2)^2 + (\omega - \omega_{10})^2} \left[\frac{\omega - \omega_{20}}{\Gamma_2/2} \right]^2 = \left(\frac{\Gamma_1}{\Gamma_2} \right)^2 \frac{\left(\omega - \omega_{10} + \frac{\omega_{10} - \omega_{20}}{\Gamma_1/2} \frac{\Gamma_1}{2} \right)^2}{(\Gamma_1/2)^2 + (\omega - \omega_{10})^2} = T_0^2 \frac{(\epsilon + f)^2}{1 + \epsilon^2}. \tag{3}$$

Here $f = 2(\omega_{10} - \omega_{20})/\Gamma$, $T_0 = \Gamma_1/\Gamma_2$, and $\epsilon = 2(\omega - \omega_{10})/\Gamma_1$. ω_{10} (ω_{20}) and Γ_1 (Γ_2) are the central frequencies and linewidths of T_1 (T_2), respectively. Equation (3) shows that the product of T_1 and T_2 with independent parameters can also produce a standard Fano line. One advantage of Eq. (3) is that the Fano line is expressed in a very clear and straight form, which makes the design of a high-contrast Fano diode flexible. For example, when the linewidths of T_1 and T_2 are determined, the Fano line can be tuned by resonant centers of ω_{10} and ω_{20}.

We know that T_1 can be exactly realized by using the element shown in Fig. 3(a), which is a waveguide inline coupled with a cavity [46,47]. Figure 3(b) shows a waveguide side coupled with a cavity, and its transmission spectrum is

$$T_2 = \frac{(\omega - \omega_{20})^2}{(\Gamma_2/2)^2 + (\omega - \omega_{20})^2} \approx \frac{(\omega - \omega_{20})^2}{(\Gamma_2/2)^2}. \tag{4}$$

The approximate equality is satisfied in the vicinity of the resonant center of $|\omega - \omega_{20}|$ less than Γ_2. Equation (4) shows that T_2 can be approximately realized using the side-coupled cavity-waveguide structure shown in Fig. 3(b).

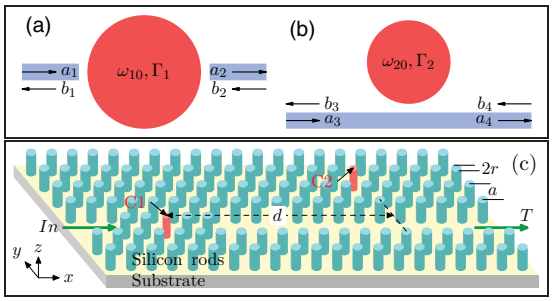

FIG. 3. (Color online) (a), (b) Schematic elements of a waveguide inline coupled (a) and side coupled (b) with a cavity to generate the response functions of T_1 and T_2, respectively. (c) Realization of (a) cascaded with (b) in a *finite* silicon photonic system. $n_a = 3.48$, $n_b = 1.0$, $r = 0.2a$ with a the lattice constant. The radius of the rod in Ci is r_i ($i = 1,2$), and the distances between C1 and C2 are d.

According to the transfer matrix method [48], the right-going wave a_i and left-going wave b_i [as shown in Figs. 3(a) and 3(b)] of the system can be related by transfer matrices,

$$\begin{pmatrix} a_4 \\ b_4 \end{pmatrix} = M_2 M_\phi M_1 \begin{pmatrix} a_1 \\ b_1 \end{pmatrix} = M \begin{pmatrix} a_1 \\ b_1 \end{pmatrix}. \tag{5}$$

Here M_1, M_2, and M_ϕ are the transfer matrix of the first element, the second element, and the free waveguide length d. They are expressed respectively as

$$M_1 = \begin{pmatrix} 1 - \frac{i\Gamma_1}{\omega-\omega_{10}} & \frac{-i\Gamma_1}{\omega-\omega_{10}} \\ \frac{i\Gamma_1}{\omega-\omega_{10}} & 1 + \frac{i\Gamma_1}{\omega-\omega_{10}} \end{pmatrix}, \tag{6}$$

$$M_\phi = \begin{pmatrix} \exp(i\phi) & 0 \\ 0 & \exp(-i\phi) \end{pmatrix}, \tag{7}$$

$$M_2 = \begin{pmatrix} 1 - \frac{\omega-\omega_{20}}{i\Gamma_2} & \frac{\omega-\omega_{20}}{-i\Gamma_2} \\ \frac{\omega-\omega_{20}}{i\Gamma_2} & 1 + \frac{\omega-\omega_{20}}{i\Gamma_2} \end{pmatrix}. \tag{8}$$

Here $\phi = \beta d_{\text{eff}}$ is the phase shift when the signal propagates from C1 to C2. β is the mode propagation constant, and d_{eff} is the effective distance between C1 and C2.

At the case of $\phi = (m + 0.5)\pi$ (m an integer), the transmission spectra of T(C1) (only when C1 exists; thin solid line), T(C2) (only when C2 exists; thin dashed line), T(C1)T(C2) (thick solid line), and T(C1,C2,ϕ) (thick dashed line) are shown in Fig. 4(a). Due to the interaction between the two cavities, T(C1)T(C2) (thick solid line) is much different from the transmission spectrum of the cascaded structure T(C1,C2,ϕ). At the case of $\phi = m\pi$ shown in Fig. 4(b),

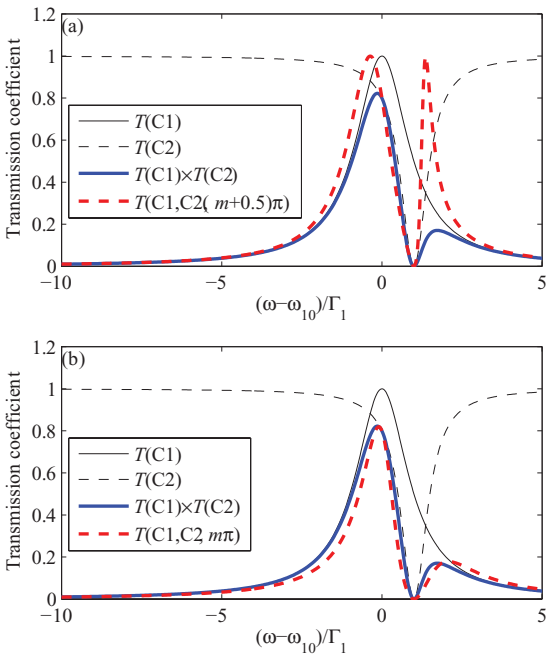

FIG. 4. (Color online) Transmission spectra of the elements shown in Figs. 3(a) and 3(b). T(C1) (thin solid line), T(C2) (thin dashed line), and T(C1,C2,ϕ) (thick dashed line) show the spectrum of C1, C2, and cascaded C1 with C2, respectively. Thick solid line shows the product of T(C1)T(C2). (a) $\phi = (m + 0.5)\pi$ with m an integer. (b) $\phi = m\pi$. At this case, T(C1,C2,ϕ) $\approx T$(C1)T(C2) can be obtained, which is the physical realization of Eq. (3).

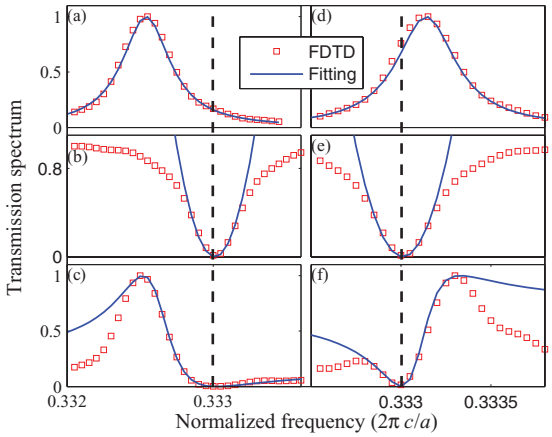

FIG. 5. (Color online) Transmission spectrum of the system shown in Fig. 3(c). The square markers are numerical results and the blue lines are fitted lines. Left (right) column, $r_1 = 0.504r$ ($r_1 = 0.503r$), $r_2 = 0.505r$, and $d = 7a$. (a), (d) Lorentzian lines of T_1 when only C1 is involved. (b), (e) Approximated parabolic lines of $T_2(\omega)$ when only C2 are involved. (c), (f) Composed Fano lines of $T = T_1 T_2$ when C1 and C2 are cascaded. The Fano factors of (c) and (f) are $f = -2$ and $f = 0.65$, respectively.

however, one can observe that T(C1)T(C2) (thick solid line) agrees well with T(C1,C2,ϕ) (thick dashed line). In this case, the response functions of C1 and C2 behave the same as they exist individually alone (i.e., interaction-free cascading), and the interaction between them seems vanishing. However, this decoupling mechanism is different from that reported in Ref. [49]. This result shows that Eq. (3), i.e., a standard Fano line, can be physically interpreted as the cascade of two resonators shown in Figs. 3(a) and 3(b) with a properly designed separation d.

Here, we use a *finite* photonic crystal (PC) structure shown in Fig. 3(c) as a numerical example. The square lattice PC is formed by silicon rods ($n_a = 3.48$) in air ($n_b = 1.0$). Using the finite difference in time domain (FDTD) method, we simulate the transmission spectrum of the system at the case of $d = 7a$, and the results are shown in Fig. 5. For the left column, $r_1 = 0.504r$ and $r_2 = 0.505r$ are selected. When C1 and C2 are introduced individually, the transmission spectra are shown in Figs. 5(a) and 5(b), respectively. Fitted curves are shown also for comparison with parameters (normalized by $2\pi c/a$) of $\omega_{10} = 0.33254$, $\Gamma_1 = 4.4 \times 10^{-4}$, $\omega_{20} = 0.33301$, and $\Gamma_2 = 5.2 \times 10^{-4}$. When C1 and C2 are introduced simultaneously, the transmission spectrum is shown in (c), which agrees well with a Fano line with parameters of $f = -2$ and $\Gamma = 4.4 \times 10^{-4}$. According to Eq. (3), the Fano factor is $f = 2(\omega_{10} - \omega_{20})/\Gamma_1 \approx -2.1$, which agrees well with the curve-fitting parameter of $f = -2$. When r_1 is tuned from $0.504r$ to $0.503r$, the results are shown on the right column of Fig. 5. The Fano factor in Fig. 5(f) changes from $f = -2.0$ to $f = 0.65$.

Apart from the asymmetrical spectrum, the field localization is also asymmetrical inherently for the left-going and right-going waves. For example, when the signal with a frequency ω_{20} is launched from right side, it will be reflected completely by C2. Then the field localization in C1 is zero.

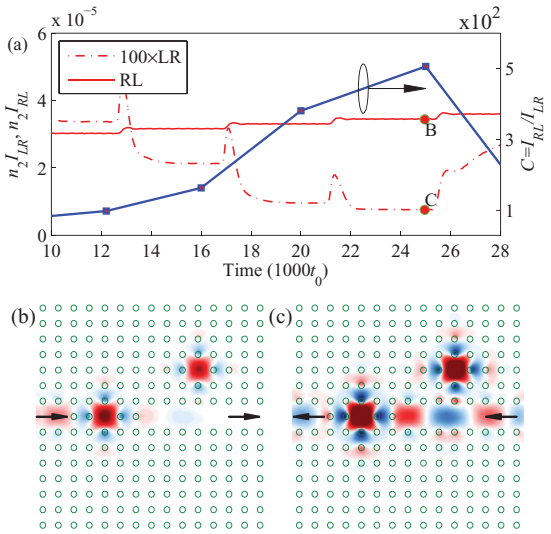

FIG. 6. (Color online) (a) Left scale: Transmission intensity I (normalized by the Kerr nonlinearity coefficient of n_2) for the LR (dash-dotted line, red online), and RL (solid line, red online) operations. $\omega_i = 0.352(2\pi c/a)$, and $t_0 = 2\pi/\omega_i$ is the period of the signal. The transmission contrast ratio (line with squares, blue online) of $C = I_{\rm LR}/I_{\rm RL}$ is shown toward the right scale. (b) and (c) respectively show the field patterns of E_z for the LR and RL operations at the points denoted by B and C in (a).

When the same signal is fed from the left side, however, the localization in C1 is not zero. When these two asymmetries (both spectrum and field localization) are combined together, an all-optical diode (AOD) with a contrast ratio tending to ∞ can be achieved in such a finite structure, based on uncoupled cavities.

The proposed SFD structure is shown in Figs. 6(b) and 6(c), which is similar to Fig. 3(c) except for the radius and refractive index of the cavity rods. The refractive index of the cavities are $n = n_0 + n_2 I$. Here $n_0 = 1.59$, n_2, and I are the linear refractive index, Kerr nonlinear coefficient, and the local light intensity inside the Kerr medium, respectively. We set $r_1 = 0.22a, r_2 = 0.223a, d = 6a$, and $\omega_i = 0.352(2\pi c/a)$. The incident $I_{\rm in}$ and transmitted intensities of LR ($I_{\rm LR}$) and RL ($I_{\rm RL}$) transmissions are all normalized by the Kerr nonlinear parameter of n_2, for the convenience in comparison.

Figure 6(a) shows the intensity profiles of the proposed SFD (in a finite size) for LR and RL operations. High contrast ratio C can be observed obviously. One can find that $T_{\rm LR}$, $T_{\rm RL}$, and C are sensitively dependent on the incident level, which is a common feature for all nonlinear structures. One can optimize the structure easily when the incident frequency and incident intensity are given. At four different incident intensities of $n_2 I_{\rm in} = [0.50, 0.51, 0.53, 0.55] \times 10^{-4}$, the LR transmissions are all greatly blocked, and the transmission intensities respectively are $n_2 I_{\rm LR} = [3.37, 2.13, 0.96, 0.76] \times 10^{-7}$. On the contrary, the transmission intensities of the RL operation are rather large, which are $n_2 I_{\rm RL} = [0.333, 0.348, 0.363, 0.379] \times 10^{-4}$. At these cases, the transmission contrast ratios of $C = I_{\rm RL}/I_{\rm LR}$ are $C = [98, 163, 380, 500]$, respectively, as shown by the line with squares (the right y scale). For the very recent AODs based on Lorentzian lines, the values of C are on the order of 10 [18,19,21–23], but we can easily achieve the contrast ratio of $C = 500$, and it is believed to be even higher if we consider a larger structure size and/or implement the optimization of chosen parameters and fine meshing. At $C = 500$, the transmission coefficients are $T_{\rm RL} = 70\%$ and $T_{\rm LR} = 0.14\%$. Figures 6(b) and 6(c) show field patterns at the states of B and C denoted in Fig. 6(a).

In summary, the state-of-the-art contrast performance of AODs (Lorentzian resonance) has been well beaten and surpassed by our distinct design mechanism of the SFD, tailoring Fano resonance in a finite silicon waveguide. Using this method, the silicon Fano diode (SFD) is designed, tuned, and realized by a cascaded inline-coupled cavity and a side-coupled cavity with proper separation. The new mechanism is independent of coupling between cavities, hence empowering tunable and reliable manipulation of directional signal transmission. The proposed SFD shows a contrast ratio tending to infinity in principle while maintaining a reasonably high unidirectional transmission. A specific example verifies that a transmission contrast ratio of larger than 500 : 1 can be achieved easily, which is at least one order higher than the state-of-the-art AOD.

Grant No. R-263-000-688-112 from the National University of Singapore is acknowledged. W.Q.D., also affiliated with the Harbin Institute of Technology, People's Republic of China, acknowledges support by the National Natural Science Foundation of China under Grant No. 11004041.

[1] E. Plum, V. A. Fedotov, and N. I. Zheludev, Appl. Phys. Lett. **94**, 131901 (2009).
[2] M. W. Feise, I. V. Shadrivov, and Y. S. Kivshar, Phys. Rev. E **71**, 037602 (2005).
[3] J. Hwang, M. H. Song, B. Park, S. Nishimura, T. Toyooka, J. W. Wu, Y. Takanishi, K. Ishikawa, and H. Takezoe, Nature Mater. **4**, 383 (2005).
[4] T. Amemiya, H. Shimizu, M. Yokoyama, P. N. Hai, M. Tanaka, and Y. Nakano, Appl. Opt. **46**, 5784 (2003).
[5] J. Fujita, M. Levy, R. M. Osgood Jr., L. Wilkens, and H. Dötsch, Appl. Phys. Lett. **76**, 2158 (2000).
[6] J. Xu, C. Cheng, M. Kang, J. Chen, Z. Zheng, Y.-X. Fan, and H.-T. Wang, Opt. Lett. **36**, 1905 (2011).
[7] K. Gallo, G. Assanto, K. R. Parameswaran, and M. M. Fejer, Appl. Phys. Lett. **79**, 314 (2001); K. Gallo and G. Assanto, J. Opt. Soc. Am. B **16**, 267 (1999).
[8] Z. Yu and S. Fan, Nature Phot. **3**, 91 (2009).
[9] N. Kono, K. Kakihara, K. Saitoh, and M. Koshiba, Opt. Express **15**, 7737 (2007).
[10] X. Zang and C. Jiang, J. Opt. Soc. Am. B **28**, 554 (2011).
[11] X. Ao, Z. Lin, and C. T. Chan, Phys. Rev. B **80**, 033105 (2009).

[12] C. He, M.-H. Lu, X. Heng, L. Feng, and Y.-F. Chen, Phys. Rev. B **83**, 075117 (2011).
[13] Z. Wang, Y. Chong, J. D. Joannopoulos, and M. Soljačić, Nature (London) **461**, 772 (2009).
[14] Y. Poo, R. X. Wu, Z. Lin, Y. Yang, and C. T. Chan, Phys. Rev. Lett. **106**, 093903 (2011).
[15] M. Scalora, J. P. Dowling, C. M. Bowden, and M. J. Bloemer, J. Appl. Phys. **76**, 2023 (1994).
[16] M. D. Tocci, M. J. Bloemer, M. Scalora, J. P. Dowling, and C. M. Bowden, Appl. Phys. Lett. **66**, 2324 (1995).
[17] F. Biancalana, J. Appl. Phys. **104**, 093113 (2008).
[18] V. Grigoriev and F. Biancalana, New J. Phys. **12**, 053041 (2010); Phot. Nano. Fund. Appl. **8**, 285 (2010).
[19] C. Zhang and Q. Niu, Phys. Rev. A **81**, 053803 (2010); S. V. Zhukovsky and A. G. Smirnov, *ibid*. **83**, 023818 (2011).
[20] S. Lepri and G. Casati, Phys. Rev. Lett. **106**, 164101 (2011).
[21] S. F. Mingaleev and Y. S. Kivshar, J. Opt. Soc. Am. B **19**, 2241 (2002).
[22] N.-S. Zhao, H. Zhou, Q. Guo, W. Hu, X.-B. Yang, S. Lan, and X.-S. Lin, J. Opt. Soc. Am. B **23**, 2434 (2006); X.-S. Lin, J.-H. Yan, J.-J. Wu, and S. Lan, Opt. Express **16**, 20949 (2008).
[23] V. Grigoriev and F. Biancalana, Opt. Lett. **36**, 2131 (2011).
[24] X. Hu, Z. Li, J. Zhang, H. Yang, Q. Gong, and X. Zhang, Adv. Funct. Mater. **21**, 1803 (2011).
[25] U. Fano, Phys. Rev. **124**, 1866 (1961).
[26] A. E. Miroshnichenko, S. Flach, and Y. S. Kivshar, Rev. Mod. Phys. **82**, 2257 (2010).
[27] B. Luk'yanchuk *et al*., Nature Mater. **9**, 707 (2010).
[28] J. A. Chen *et al*., Science **328**, 1135 (2010).
[29] V. Giannini *et al*., Nano Lett. **11**, 2835 (2011).
[30] F. Hao *et al*., Nano Lett. **8**, 3983 (2008).
[31] N. Verellen *et al*., Nano Lett. **9**, 1663 (2009).
[32] S. Zhang, K. Bao, N. J. Halas, H. Xu, and P. Nordlander, Nano Lett. **11**, 1657 (2011).
[33] M. Rahmani *et al*., Nanotechnology **22**, 245204 (2011).
[34] C. P. Holfeld *et al*., Phys. Rev. Lett. **81**, 874 (1998).
[35] S. Fan, Appl. Phys. Lett. **80**, 908 (2002).
[36] A. E. Miroshnichenko and Y. S. Kivshar, Opt. Express **13**, 3969 (2005).
[37] M. V. Rybin *et al*., Phys. Rev. Lett. **103**, 023901 (2009).
[38] S. Fan, W. Suh, and J. D. Joannopoulos, J. Opt. Soc. Am. A **20**, 569 (2003).
[39] H. Yang *et al*., Appl. Phys. Lett. **95**, 023110 (2009).
[40] F. Patthey, M. H. Schaffner, W. D. Schneider, and B. Delley, Phys. Rev. Lett. **82**, 2971 (1999).
[41] Y.-F. Xiao, M. Li, Y.-C. Liu, Y. Li, X. Sun, and Q. Gong, Phys. Rev. A **82**, 065804 (2010).
[42] A. R. Cowan and J. F. Young, Phys. Rev. E **68**, 046606 (2003).
[43] S. F. Mingaleev, A. E. Miroshnichenko, and Y. S. Kivshar, Opt. Express **16**, 11647 (2008).
[44] A. E. Miroshnichenko *et al*., Phys. Rev. A **79**, 013809 (2009).
[45] A. E. Miroshnichenko and Y. S. Kivshar, Phys. Rev. E **72**, 056611 (2005).
[46] Y. Xu, Y. Li, R. K. Lee, and A. Yariv, Phys. Rev. E **62**, 7389 (2000).
[47] S. Fan, P. R. Villeneuve, J. D. Joannopoulos, M. J. Khan, C. Manolatou, and H. A. Haus, Phys. Rev. B **59**, 15882 (1999).
[48] H. A. Haus and Y. Lai, J. Lightwave Technol. **9**, 754 (1991).
[49] C.-M. Tsai and C.-P. Lee, IEEE J. Quantum Electron. **34**, 427 (1998).